Identification of Glycosylation-Related Gene Signatures in Astrocytes from Glaucoma Using GEO Datasets

Dingqiao Wang^{1,3}, Minyi Zhu², Peidong Yuan², Yiyu Xie², Bingying Lin³, Hongzhi Yuan^{2,*}

¹Department of Ophthalmology, the Eighth Affiliated Hospital, Sun Yat-Sen University, Shenzhen,

China

²Department of Ophthalmology, the Seventh Affiliated Hospital, Sun Yat-Sen University, Shenzhen, China

³State Key Laboratory of Ophthalmology, Zhongshan Ophthalmic Center, Sun Yat-sen University; Guangdong Provincial Key Laboratory of Ophthalmology and Visual Science; Guangdong Provincial Clinical Research Center for Ocular Diseases, Guangzhou, 510060, China. *Corresponding Author

Abstract: Glycosylation critically regulates folding, stability, and signaling in neurodegenerative disorders; however, its role in glaucoma pathogenesis remains underexplored. We aimed investigate differentially expressed glycosylation-related genes (GRGs) and glaucoma astrocytes explore their connections with immune responses, an aspect that has not been systematically addressed in prior computational studies. We integrated two glaucoma-related microarray datasets (GSE2378 and GSE9944) comprising 13 glaucoma and 42 control human astrocyte samples. Differential expression analysis and functional enrichment assessments were conducted using standard bioinformatics approaches. We developed protein-protein interaction networks, identified essential genes, and evaluated immune-related gene expression through single-sample Gene Set Enrichment Analysis (GSEA). The study identified 42 differentially expressed GRGs and seven hub genes (SEC23A, BET1, ARCN1, COPB2, VCP, UBC, and SEC61B) involved in protein trafficking and secretory pathway **Functional** regulation. analysis revealed glycoprotein significant enrichment in metabolic processes and inflammatory pathways. GSEA highlighted the involvement of Wnt/β-catenin signaling and interleukin-23 pathways. Six hub genes demonstrated substantial diagnostic capacity. Analysis of Immune cell infiltration revealed significant alterations in eight immune cell populations, with activated CD4+ T cells showing positive correlations with all hub genes. These findings suggest that astrocyte glycosylation

contributes to glaucoma progression and may be associated with immune dysregulation, providing new insights into disease pathogenesis identifying potential and diagnostic biomarkers and therapeutic targets.

Keywords: Glaucoma; Glycosylation-Related Genes; Bioinformatics; Immune Cell Infiltration; Astrocyte Dysfunction

1. Introduction

Glaucoma represents one of the leading causes of irreversible blindness worldwide, featuring the gradual degeneration of retinal ganglion cells (RGCs) and optic nerve pathology [1]. Recent research has highlighted that in addition to the loss of RGCs, other cells such as astrocytes contribute significantly to glaucoma pathogenesis [2]. These cells contribute toward neuroinflammation and disrupt the balance of the retinal microenvironment. However, the precise molecular pathways driving astrocyte impairment in glaucoma remain unclear.

Growing evidence demonstrates that astrocytes significantly involved in glaucoma pathogenesis. Previous study of glaucomatous tissues have revealed that glial cell activation predominantly affects astrocytes, accounting for 62.5% observed glial changes[3]. Glycosylation, an essential post-translational modification, plays crucial roles in protein folding, cellular signaling, and immune regulation[4]. In central nervous system diseases such as Alzheimer's disease and Parkinson's disease, astrocyte glycosylation has been shown critical for maintaining homeostasis, regulating signal transduction pathways, and modulating neuroinflammatory responses [5]. Studies have demonstrated that glycosylation dysfunction leads to protein aggregation, Golgi fragmentation, and altered protein processing, thereby contributing to neurodegeneration [6-7]. However, the specific involvement of glycosylation-related genes (GRGs) in astrocyte dysfunction during glaucoma progression remains unexplored. Despite extensive re-analyses ofpublic glaucoma datasets focusing on various molecular mechanisms, no systematic investigation has specifically examined astrocyte glycosylation machinery or its immunological implications in human glaucoma, representing a critical knowledge gap.

Although glycosylation modifications play important roles in neurodegenerative diseases, their specific involvement in glaucoma astrocyte dysfunction remains unclear. This study aims to address three key questions: glycosylation-related genes are differentially expressed in glaucoma astrocytes, what biological pathways are involved, and how these changes relate to immune microenvironment alterations. We hypothesize glycosylation-related genes are dysregulated in glaucoma astrocytes and associated with protein processing pathways and immune infiltration patterns.

This study integrates two microarray datasets with batch effect correction and combines glycosylation gene screening with immune infiltration analysis. We performed functional enrichment analyses to reveal the biological genes, mechanisms associated with these identified critical hub genes protein-protein interaction network analysis, and assessed immune-related gene expression signatures to understand glycosylation-immune interactions. This work provides the first investigation of glycosylation systematic machinery in human glaucoma astrocytes, establishing a theoretical foundation for understanding glycosylation's role in glaucoma pathogenesis and identifying potential biomarkers.

2. Material and Methods

2.1 Data Source and Processing

Our analysis incorporated glaucoma-relevant transcriptomic data from the GSE2378[8-10](Hernandez et al., 2002;

Kompass et al., 2008; Nikolskaya et al., 2009) and GSE9944[11](Lukas et al., 2008) datasets retrieved from the GEO database. Data acquisition and preliminary processing were conducted using R (The R Foundation for Statistical Computing, Vienna, Austria) using GEOquery v2.70.0[12] (Barrett et al., 2013; Davis S). Both datasets consist of samples obtained from human astrocytes. The GSE2378 dataset, which employs the GPL8300 platform, includes seven glaucoma cases and six healthy controls. The GSE9944 dataset, based on the GPL571 platform, comprised 6 glaucoma samples and 36 control samples, as shown in Table 1. All samples from both the glaucoma and control groups were included in the analyses conducted in this investigation.

Table 1. GEO Microarray Chip Information

	GSE2378	GSE9944
Platform	GPL8300	GPL571
Species	Homo sapiens	Homo sapiens
Tissue	Astrocytess	Astrocytes
Samples in Glaucoma group	7	6
Samples in Control group	6	36
Reference	PMID:11921203 PMID:18822132 PMID:19426536	PMID:186139 64

GEO, Gene Expression Omnibus.

2.2 GRG Curation

The GRGs were comprehensively compiled using two integrated approaches. First, we investigated the GeneCards[13](Stelzer et al., 2016) knowledge repository using "Glycosylation" as our query parameter and identified 326 protein-coding genes with relevance metrics exceeding 9. Second, a systematic literature review of PubMed revealed an additional 282 genes[14](Chen et al., 2022). After eliminating duplicates, a final total of 518 unique GRGs was established for further analysis, as detailed in Supplementary Table 1.

2.3 Batch effect Removal and Quality Control

The consolidated dataset, comprising 13 diseased specimens and 42 healthy controls, was established through integration of GSE2378 and GSE9944 data. Batch effect correction was implemented using the sva software package (version 3.50.0) [15](Leek et al., 2012). Following this step, data standardization and

probe mapping were conducted via the limma analytical package (version 3.58.1) [16](Ritchie et al., 2015). To evaluate sample distribution characteristics both pre- and post-correction, we applied dimensionality reduction through PCA[17] (Ben Salem and Ben Abdelaziz, 2021), a computational method that simplifies complex datasets by identifying key components from high-dimensional information, enabling data representation in reduced dimensions. This approach supports effective visualization in two or three dimensional space, thereby clearly revealing the fundamental properties of the dataset.

2.4 Identification of Glycosylation-Related Differentially Expressed Genes (DEGs)

DEGs was assessed across the merged dataset using the "limma" package (version 3.58.1) [16](Ritchie et al., 2015) to compare transcriptomic patterns between glaucoma and control samples. We applied a threshold of |logFC| > 0 with a false discovery rate (FDR) < 0.05 to identify DEGs. This inclusive approach was chosen to capture subtle but statistically significant transcriptional changes in purified astrocyte populations, where modest expression alterations may represent important regulatory mechanisms in glaucoma pathogenesis. Genes were considered DEGs if they had an absolute fold change exceeding 0, with a false discover rate (FDR) of <0.05. Transcripts showing positive fold changes (log fold change [logFC] > 0, FDR < 0.05) were designated as upregulated, whereas those with negative fold changes (logFC < 0, FDR < 0.05) were designated as downregulated. The distribution of these DEGs displayed through a volcano visualization created using the "ggplot2" package (version 3.4.4).

To determine the glycosylation-related DEGs relevant to glaucoma, we compared the identified DEGs (|logFC| > 0 and adjusted p < 0.05) from the combined dataset with our previously established list of GRGs. This intersection was illustrated using a Venn diagram. The expression profiles of the resulting glycosylation-related DEGs were visualized using a hierarchical clustering heatmap generated via the "pheatmap" package (version 1.0.12).

2.5 Gene Ontology (GO) and Kyoto Encyclopedia of Genes and Genomes (KEGG)

Pathway Enrichment Analysis

Functional enrichment of evaluation glaucoma-related DEGs was performed using "clusterProfiler" (version 4.10.0) [18](Yu et al., 2012). The analytical framework encompassed categorization[19](Mi et al., 2019). Enrichment significance was established using statistical parameters of adjusted p-value of <0.05, combined with an FDR cutoff of 0.25. Furthermore, we performed KEGG pathway analysis to identify biological pathways [20](Kanehisa and Goto, 2000). The enriched pathways were visualized using the "Pathview" package (version 1.42.0)[21](Luo and Brouwer, 2013), which illustrates molecular interactions and biological networks. The significance thresholds for the pathway enrichment analysis were consistent with those used in the GO analysis.

2.6 Gene Set Enrichment Analysis (GSEA)

GSEA(Subramanian et al., 2005) was performed to examine the distribution characteristics of predefined gene sets within ranked gene lists associated with specific phenotypes, enabling the evaluation of their contributions to different phenotypes. Initially, genes from our integrated dataset were ordered based on their logFC values by employing a comprehensive gene expression profile. The evaluation was performed using the "clusterProfiler" package (version 4.10.0)[22](Yu et al., 2012), with configuration parameters including a random seed of 2020, 1,000 permutations, and gene set size limitations spanning from 10 to 500 genes.

We used the Molecular Signatures Database c2.cp.all.v2022.1. Hs.symbols.gmt, which includes a comprehensive collection of canonical pathways, totaling 3,050 gene sets. To assess statistical significance, we established the criteria of adjusted p-values below 0.05, and an FDR q-value of <0.25. Normalized enrichment scores and their corresponding significance values were calculated to identify pathways that were significantly associated with glaucoma.

2.7 PPI Network Construction and Hub Gene Identification

The PPI network was established using the STRING database(Szklarczyk et al., 2019), with a minimal interaction score cutoff of 0.4. Subsequently, network evaluation was conducted using Cytoscape software (version 3.8.2; Institute for Systems Biology, Seattle, WA,

USA)[23](Shannon et al., 2003), employing the "cytoHubba"[24](Chin et al., 2014) plugin to determine hub genes among the previously characterized DEGs.

2.8 Construction of Regulatory Networks (Transcription Factor [TF]-mRNA and Micro [mi]RNA-mRNA)

To explore the regulatory mechanisms linked to the identified hub genes, we established two types of regulatory networks: TF-mRNA and miRNA-mRNA. Using the ChIPBase database[25](Zhou et al., 2017), we identified transcription factors that may regulate glycosylation-related DEGs. Connections among regulatory proteins and downstream targets were mapped through Cytoscape software [23](Shannon et al., 2003), which allowed for the construction of a comprehensive TF-mRNA regulatory network.

Additionally, to examine post-transcriptional regulation, we analyzed miRNA-mRNA interactions using the StarBase v3.0 database[26](Li et al., 2014). This analysis led us to identify miRNAs associated with glycosylation-related DEGs. and we subsequently miRNA-mRNA created an regulatory network using Cytoscape effectively illustrate these interactions.

2.9 Validation of Hub Gene Expression

To assess the biological relevance of the identified hub genes, we performed expression comparison of glaucoma and control samples from GSE2378 and GSE9944. We visualized the expression patterns of these hub genes using box plots, which effectively illustrated the distribution of expression levels.

2.10 Diagnostic Performance Analysis

Diagnostic performance of core genes was evaluated through ROC analysis via pROC package (v1.18.5) [27](Robin et al., 2011). The area under the curve (AUC) was computed for each hub gene to quantify its capacity in distinguishing patients with glaucoma from healthy controls. We established interpretation guidelines for diagnostic accuracy based on AUC thresholds: superior diagnostic capability was indicated by AUC scores of 0.9–1.0, while moderate discriminatory power corresponded to values of 0.7–0.9, and limited diagnostic utility was reflected by scores of 0.5–0.7. This analytical approach yielded a quantitative

validation, demonstrating the prospective utility of these pivotal genes as diagnostic markers of glaucoma.

2.11 Single-Sample GSEA (ssGSEA)

We conducted ssGSEA to evaluate immune-related gene expression signatures within astrocyte samples, aiming to explore the potential associations between astrocytes and immune regulatory mechanisms at the transcriptional level[28] (Xiao et al., 2020). This method evaluated immune transcriptional signatures across multiple cell types. Enrichment scores generated a matrix reflecting molecular immune signatures within astrocytes.

This analytical approach enabled the assessment of immune-associated transcriptional programs corresponding to multiple immune cell subsets, including activated CD8+ T lymphocytes, stimulated dendritic cells, gamma delta T cells, natural killer cells, and regulatory T cells. Enrichment scores were calculated to create an immune-related gene expression matrix that represented immune-associated molecular changes within astrocytes rather than actual immune cell infiltration.

2.12 Differential Immune Cell Analysis

We performed a comparative assessment of immune-related gene expression signatures between glaucoma specimens and healthy controls using the "ggplot2" package (version 3.4.4). This evaluation identified distinct immune-associated transcriptional within astrocytes that exhibited statistically significant variations between the experimental cohorts, which were subsequently chosen for additional correlation examinations. investigate the interrelationships among these immune-related gene signatures, we applied Spearman's rank correlation methodology, with the findings displayed using the "pheatmap" package (version 1.0.12).

2.13 Hub Gene-Immune Cell Correlation Analysis

Relationships among hub genes and immune cells were assessed by Spearman's correlation analysis. Only the correlations that achieved statistical significance (p < 0.05) were retained and illustrated through bubble plots created using the "ggplot2" package (version 3.4.4).

3. Results

3.1 Study Design and Workflow

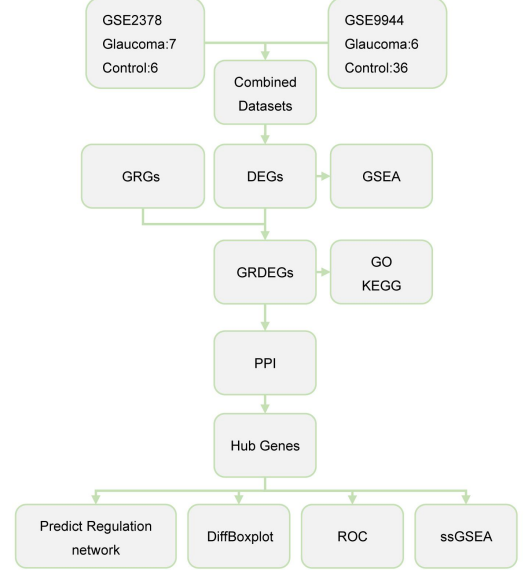


Figure 1. Schematic Workflow of the Study Design

The analysis pipeline includes data integration, differential expression analysis, identification of glycosylation-related DEGs, functional enrichment analyses (GO, KEGG, and GSEA), protein-protein interaction network analysis, hub gene identification, expression validation, and immune cell infiltration analysis. GO: Gene Ontology; KEGG: Kyoto Encyclopedia of Genes and Genomes; GSEA: Gene Set Enrichment Analysis; PPI: Protein-Protein Interaction; ROC:

Receiver Operating Characteristic; ssGSEA: Single-Sample Gene Set Enrichment Analysis.

To comprehensively investigate the roles of glycosylation-associated genes in glaucoma pathogenesis, we developed an integrated bioinformatics pipeline (Figure 1). analytical framework commenced with the concurrent extraction of GRGs and DEGs from glaucoma-associated consolidated Through the intersection of these genetic signatures, we identified glycosylation-related DEGs. Subsequently, we executed analytical streams and functional annotation analysis incorporating GO terms and KEGG pathway mapping to elucidate the biological relevance of glycosylation-related DEGs, while applied **GSEA** was across the entire transcriptomic landscape. Subsequently, we constructed PPI networks to identify central hub These pivotal genes comprehensively evaluated using four distinct methodological approaches: construction of regulatory circuits incorporating TFs and miRNAs, comparative expression profiling, ROC curve assessment for diagnostic capability and correlation analysis with evaluation. immune cell infiltration dynamics through ssGSEA.

3.2.Integration and Batch Effect Removal of Glaucoma Datasets

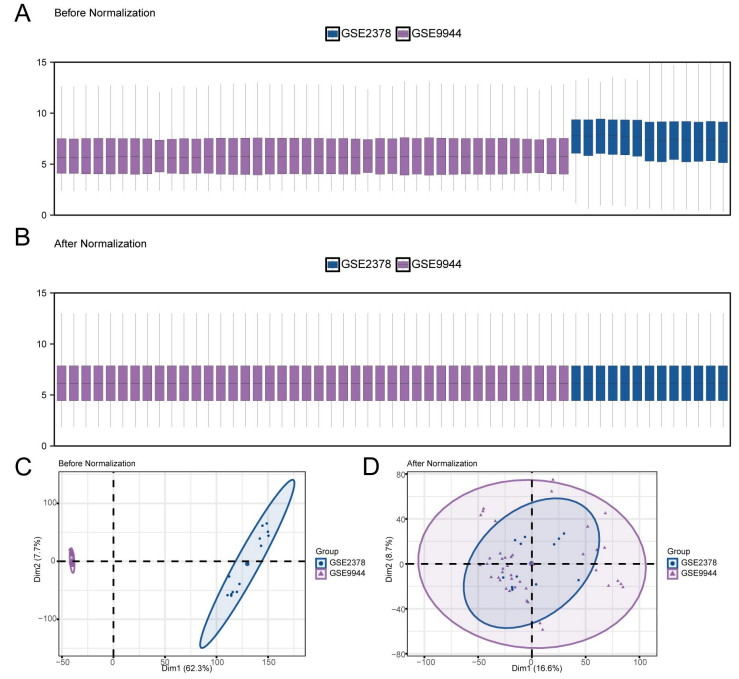


Figure 2. Assessment of Batch Effect Removal in Integrated Glaucoma Datasets.

(A) Box plots showing gene expression distribution before batch effect removal. (B) Box

plots demonstrating normalized expression distribution after batch effect removal. (C)

Principal Component Analysis (PCA) plot before batch effect removal, showing distinct clustering by dataset. (D) PCA plot after batch effect removal, showing improved integration of datasets. Blue represents samples from GSE2378 and purple represents samples from GSE9944.

We merged GSE2378 and GSE9944 microarray datasets utilizing "sva" package for batch correction. Correction efficacy was evaluated through expression distribution analysis and dimensionality reduction approaches. Box plots

illustrated gene expression patterns pre- and post-correction (Figure 2A, B). Additionally, PCA was applied to assess sample clustering characteristics (Figure 2C, D). Results from both visualization methods confirmed effective batch correction across all specimens in the consolidated dataset.

3.3 Identification of Glycosylation-Related DEGs

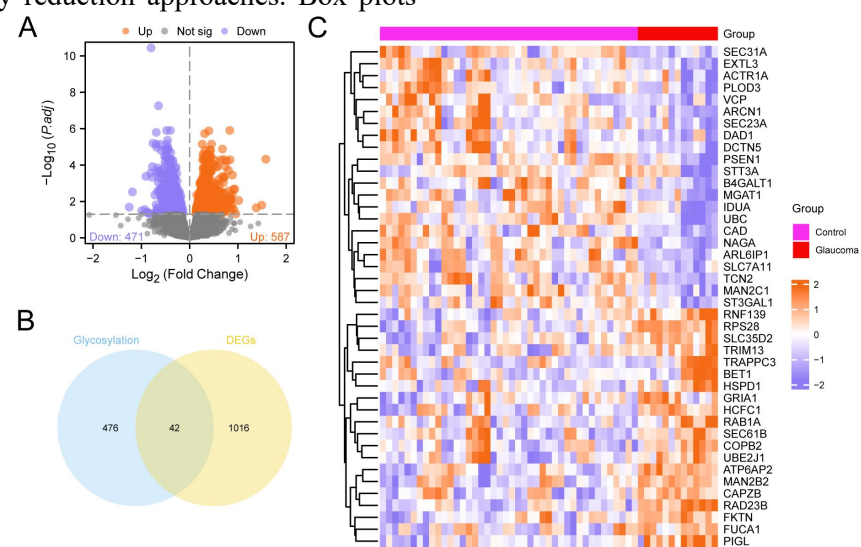


Figure 3. Identification of Glycosylation-Related Differentially Expressed Genes in Glaucoma.

(A) Volcano plot showing the distribution of differentially expressed genes between glaucoma and control samples. (B) Venn diagram illustrating the intersection between differentially expressed genes (DEGs) and glycosylation-related genes (GRGs) derived from GeneCards database (518 total genes, see Table Supplementary 1) to identify Glycosylation-related DEGs. (C) Heatmap showing the expression patterns of 42 identified Glycosylation-related DEGs across glaucoma (orange-red) and control (pink-purple) samples. Orange indicates high expression and blue indicates low expression in the heatmap.

We performed differential gene expression profiling of the consolidated dataset by comparing glaucoma specimens with healthy control samples using the "limma" package. This computational approach revealed a comprehensive set of 1,058 DEGs satisfying the selection criteria of $|\log FC| > 0$, combined with an adjusted p-value of <0.05. Within this gene signature, 587 transcripts were upregulated ($\log FC > 0$, adj. p < 0.05), whereas 471 were downregulated ($\log FC < 0$, adj. p < 0.05). The distribution of the expression patterns of these

DEGs was visualized using a volcano plot (Figure 3A).

To further investigate glycosylation-specific changes in glaucoma, we performed a Venn diagram analysis to determine the overlap between the DEGs (|logFC| > 0, adj. p < 0.05) and our curated list of GRGs (Figure 3B). The GRGs comprised 518 genes derived from GeneCards database (keyword: "Glycosylation", protein-coding genes, Relevance score > 9, yielding 326 genes) and published work (282 genes) (Chen et al., 2022), with duplicates removed (complete gene list in Supplementary Table 1). This analysis revealed 42 DEGs associated with glycosylation, including ACTR1A. ARCN1, ARL6IP1, ATP6AP2, B4GALT1, BET1, CAD, CAPZB, COPB2, DAD1, DCTN5, EXTL3, FKTN, FUCA1, GRIA1, HCFC1, HSPD1, IDUA, MAN2B2, MAN2C1, MGAT1, NAGA, PIGL, PLOD3, PSEN1, RAB1A, RAD23B, RNF139, RPS28, SEC23A, SEC31A, SEC61B, SLC35D2, SLC7A11, ST3GAL1, STT3A, TCN2, TRAPPC3, TRIM13, UBC, UBE2J1, and VCP. We analyzed and visualized expression patterns of glycosylation-related DEGs across different

sample groups using a hierarchical clustering heatmap created using the "pheatmap" package (Figure 3C).

3.4.Functional Enrichment Analysis of Glycosylation-Related DEGs

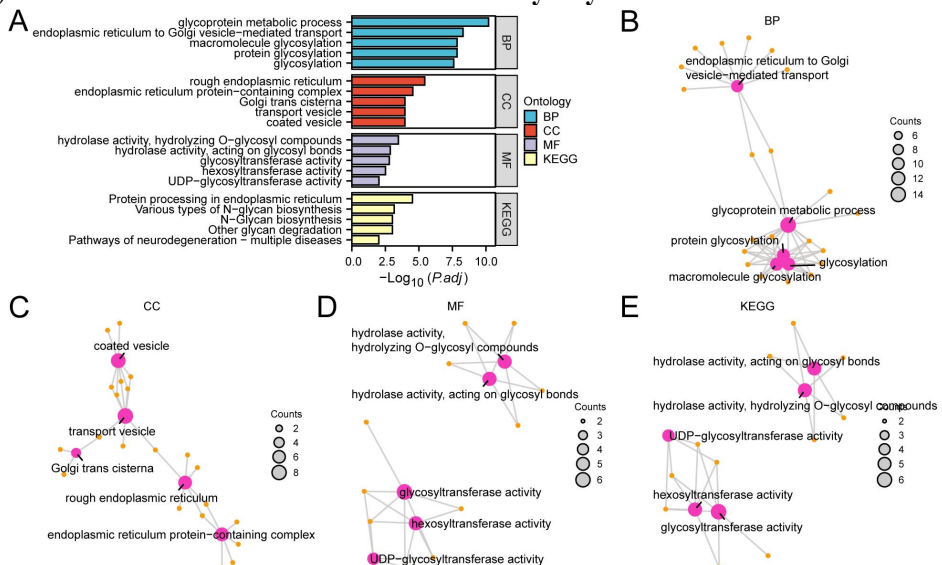


Figure 4. GO and KEGG Enrichment Analysis for of Glycosylation-Related Differentially Expressed Genes

(A) Bar plot showing significantly enriched GO terms and KEGG pathways, with bar length representing-log10 (adjusted p-value). (B-E) Network visualization of enriched terms in biological process (B), cellular component (C), molecular function (D), and KEGG pathways (E). Pink nodes represent enrichment terms, orange nodes represent genes, and connecting lines indicate relationships. Node size corresponds to the number of associated genes. All analyses were performed with thresholds of adj.p < 0.05 and FDR < 0.25.

To systematically explore the distribution patterns of glycosylation-related DEGs across broader biological processes and signaling pathways beyond their known glycosylation functions, we employed systematic functional annotation using GO databases and KEGG resources. Our investigation encompassed 42 glycosylation-related DEGs and identified substantial enrichment patterns across diverse biological mechanisms and metabolic networks, adhering to rigorous statistical thresholds with corrected p-values of <0.05, and FDR maintained below 0.25 (Table 2). Functional through categorization GO analysis that these demonstrated genes exhibited preferential involvement in fundamental cellular mechanisms, with particular emphasis on the protein glycosylation machinery transmembrane trafficking processes. The most significantly enriched biological process terms

included glycoprotein metabolism, ER-to-Golgi vesicular trafficking, macromolecular modification. and protein glycosylation processes. Regarding cellular components, the analysis highlighted strong associations with key organelles involved in protein modification and trafficking, particularly the rough ER, ER protein-containing complexes, Golgi trans cisternae, transport vesicles, and coated vesicles. Regarding molecular functions, glycosylation-related DEGs showed significant enrichment in activities crucial for glycosylation, including hydrolase activity that specifically hydrolyzes O-glycosyl compounds, hydrolase activity targeting glycosyl bonds. glycosyltransferase activity, hexosyltransferase activity, and uridine diphosphate-glycosyltransferase activity.

KEGG pathway analysis further supported our findings, revealing gene involvement in critical processes including ER protein processing, N-glycan biosynthetic pathways, glycan degradation, and neurodegeneration-associated networks. Enrichment results for functional categories and molecular pathways are displayed in bar graph format (Figure 4A). Network visualizations were constructed to illustrate relationships across biological gene-term processes (Figure 4B), cellular components (Figure 4C), molecular functions (Figure 4D), and metabolic pathways (Figure 4E). In these representations, network connecting

indicate associations between molecules and functional categories, while node size reflects the gene count for each term.

3.5 Gene Set Enrichment Analysis

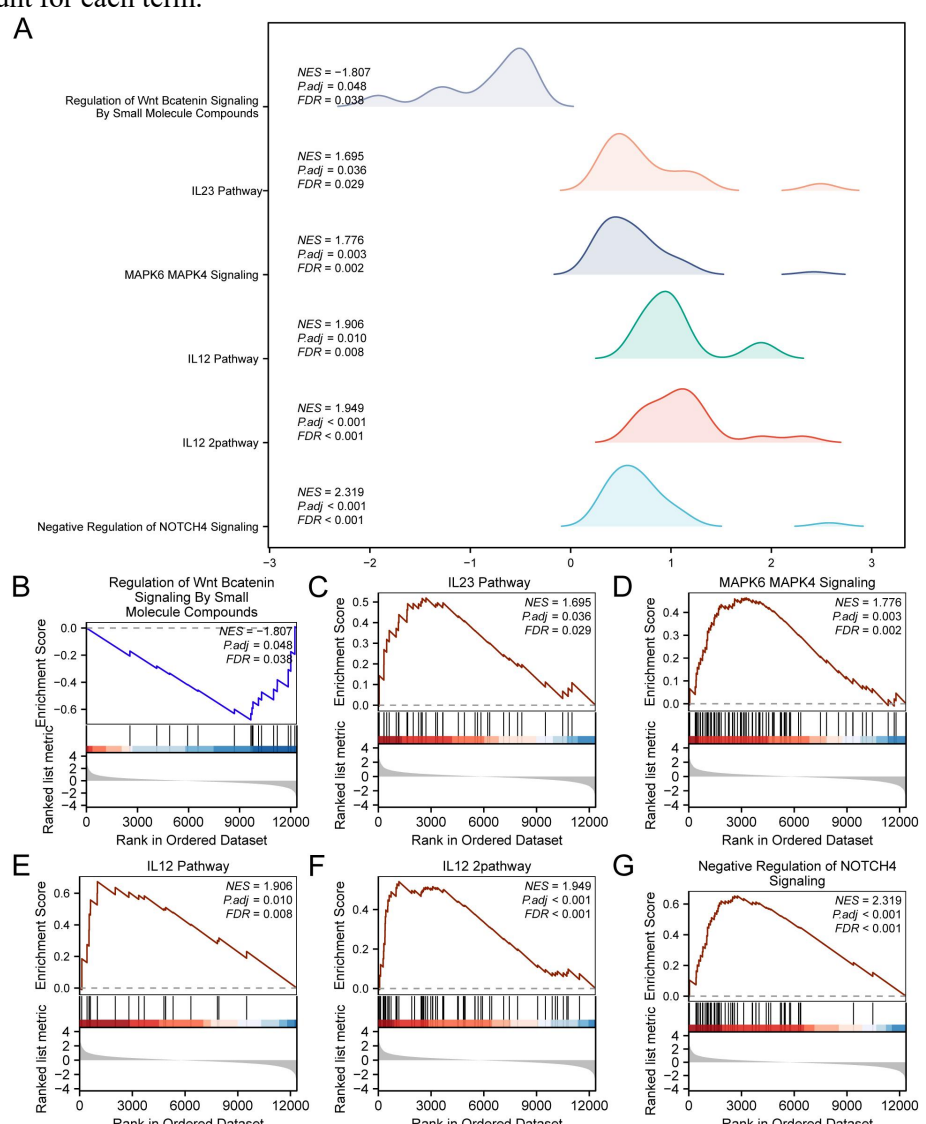


Figure 5. Gene Set Enrichment Analysis of Glaucoma-Associated Pathways.

(A) Overview of enrichment plots showing seven significantly enriched biological pathways. (B-G) Individual enrichment plots for key pathways: Wnt/β-catenin signaling regulation (B), IL-23 pathway (C), MAPK6/MAPK4 signaling (D), IL-12 pathway (E), IL-12 secondary pathway (F), and negative regulation of NOTCH4 signaling (G). All pathways shown met the significance criteria of adj.p < 0.05 and FDR < 0.25.

To assess the functional implications of transcriptomic alterations across the entire genome in glaucoma pathogenesis, we implemented GSEA using integrated transcriptional profiles derived from our consolidated dataset. This analytical approach facilitated the comprehensive exploration of

diverse cellular mechanisms, subcellular compartments, and biochemical pathways linked to the complete spectrum of expressed transcripts, extending beyond the exclusive examination of differentially regulated genes (Figure 5A and Table 3).

GSEA revealed significant enrichment (adjusted p < 0.05, FDR < 0.25) in several key signaling pathways and biological functions. Notably, the analysis showed substantial enrichment in the modulation of Wnt/β-catenin signaling through small molecule compounds (Figure 5B), the interleukin (IL)-23 pathway (Figure 5C), and the mitogen-activated protein kinase (MAPK)6/MAPK4 signaling pathways (Figure 5D). Furthermore, we identified two distinct IL-12 signaling cascades (Figure 5E, F) and

observed the negative regulation of neurogenic locus notch homolog protein 4 signaling (Figure 5G), indicating intricate interactions among the pathways involved in the pathogenesis of

glaucoma.

3.6 PPI Network Analysis and Hub Gene Identification

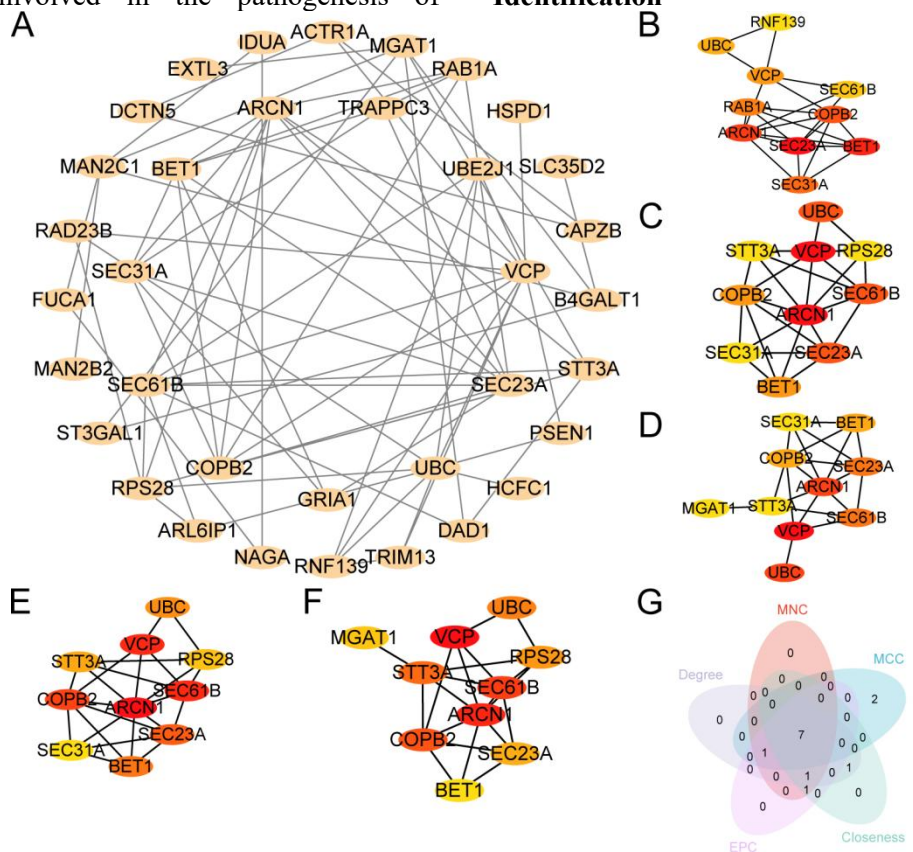


Figure 6. Protein-Protein Interaction Network Analysis and Hub Gene Identification.

(A) PPI network of Glycosylation-related DEGs constructed using STRING database. (B-F) Top 10 ranked genes identified by different topological algorithms: MCC (B), MNC (C), Degree (D), EPC (E), and Closeness (F). Node colors transition from red to yellow indicating decreasing importance scores. (G) Venn diagram showing the intersection of top 10 ranked genes across all five algorithms, identifying seven consensus hub genes. Glycosylation-related Glycosylation-Related DEGs: Differentially Expressed Genes: PPI: Protein-Protein Interaction Network.

An interaction network among the 42 glycosylation-related DEGs was established using the STRING database (Figure 6A). The analysis of this network showed significant interactions among 35 of the glycosylation-related DEGs, which included ACTRIA, MGATI, RABIA, HSPDI, SLC35D2, CAPZB, B4GALTI, STT3A, PSENI, HCFC1, DADI, TRIM13, RNF129, NAGA, ARL6IP1, RPS28, ST3GAL1, MAN2B2, FUCAI, RAD23B, MAN2C1, DCTN5, EXTL3, IDUA, TRAPPC3,

UBE2J1, VCP, SEC23A, UBC, GRIA1, COPB2, SEC61B, SEC31A, BET1, and ARCN1.

To identify the most crucial genes within this network, we utilized five different topological analysis algorithms using the "cytoHubba" plugin in Cytoscape: MCC, MNC, Degree, EPC, and Closeness. The top ten genes identified by each algorithm are represented in separate networks (Figure 6B-F), with the transition of node colors from red to vellow indicating decreasing importance scores. Through intersection analysis of the top-ranked genes from all five algorithms (Figure 6G), we successfully identified seven consistent hub genes: SEC23A, BET1, ARCN1, COPB2, VCP, UBC, and SEC61B.

3.7 Construction of Hub Gene Regulatory Networks

(A) mRNA-TF regulatory network. Orange nodes represent hub genes (mRNA), and purple nodes represent transcription factors. (B) mRNA-miRNA regulatory network. Orange nodes represent hub genes (mRNA), and green

nodes represent miRNAs. TF: Transcription Factor

To explore the regulatory mechanisms of the key genes, we created two distinct types of regulatory networks using various databases. First, we utilized the ChIPBase database to identify transcription factors associated with hub

genes, which allowed us to construct an mRNA-TF regulatory network. This network, visualized using the Cytoscape software (Figure 7A), included five glycosylation-related DEGs and 28 transcription factors, and their interactions are detailed in Supplementary Table 2

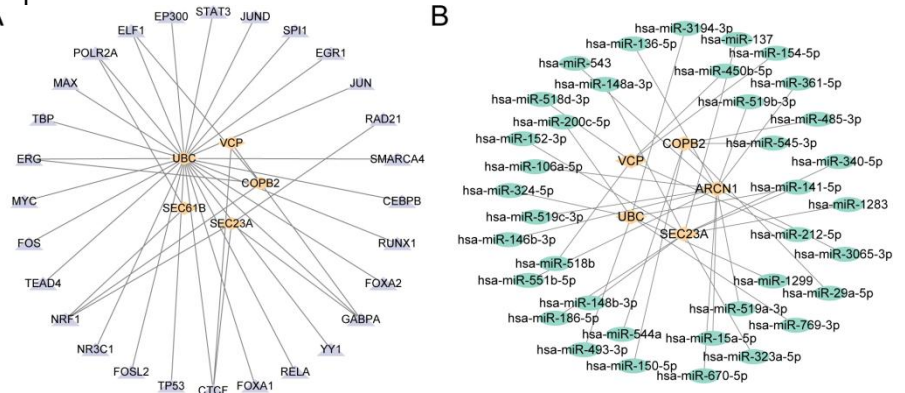


Figure 7. Regulatory Network Analysis of Hub Genes.

Table 2. Results of GO and KEGG Enrichment Analysis for Glycosylation-Related DEGs

Ontology	ID	Description	GeneRatio	BgRatio	pvalue	p.adjust
BP	GO:0009100	glycoprotein metabolic process	14/42	386/18800	5.87e-14	6.5e-11
BP	GO:0006888	endoplasmic reticulum to Golgi vesicle-mediated transport	9/42	129/18800	9.36e-12	5.18e-09
BP	GO:0006486	protein glycosylation	10/42	225/18800	5.2e-11	1.44e-08
BP	GO:0043413	macromolecule glycosylation	10/42	225/18800	5.2e-11	1.44e-08
BP	GO:0070085	glycosylation	10/42	244/18800	1.15e-10	2.55e-08
CC	GO:0005791	rough endoplasmic reticulum	6/42	79/19594	1.65e-08	3.66e-06
CC	GO:0140534	endoplasmic reticulum protein-containing complex	6/42	125/19594	2.6e-07	2.87e-05
CC	GO:0030133	transport vesicle	8/42	402/19594	1.88e-06	0.0001
CC	GO:0000138	Golgi trans cisterna	3/42	12/19594	1.99e-06	0.0001
CC	GO:0030135	coated vesicle	7/42	290/19594	2.51e-06	0.0001
		()-glycosyl compounds	5/42	94/18410	2.28e-06	0.0003
MF	GO:0016798	hydrolase activity, acting on glycosyl bonds	5/42	144/18410	1.84e-05	0.0014
MF	GO:0016757	glycosyltransferase activity	6/42	271/18410	3.24e-05	0.0016
MF	GO:0016758	hexosyltransferase activity	5/42	198/18410	8.42e-05	0.0031
MF	GO:0008194	UDP-glycosyltransferase activity	4/42	144/18410	0.0003	0.0094
KEGG		Protein processing in endoplasmic reticulum	8/35	171/8164	4.57e-07	3.02e-05
KEGG	hsa00513	Various types of N-glycan biosynthesis	4/35	39/8164	2.09e-05	0.0007
KEGG	hsa00511	Other glycan degradation	3/35	18/8164	5.64e-05	0.0009
KEGG	hsa00510	N-Glycan biosynthesis	4/35	50/8164	5.67e-05	0.0009
KEGG		Pathways of neurodegeneration - multiple diseases	8/35	476/8164	0.0007	0.0097

GO, Gene Ontology; BP, Biological Process; CC, Cellular Component; MF, Molecular Function; KEGG, Kyoto Encyclopedia of Genes and Genomes; DEGs, Differentially Expressed Genes.

Next, we developed an mRNA-miRNA regulatory network by leveraging the StarBase database to identify miRNAs that correlated with hub genes. This network was also visualized using Cytoscape (Figure 7B) and showed

interactions between the same 5 (comprehensive interaction data available in glycosylation-related DEGs and 37 miRNAs Supplementary Table 3).

Table 3. Results of GSEA for Combined Datasets

ID	setSize	enrichmentScore	NES	pvalue	p.adjust	qvalue	rank
REACTOME_NEGATIVE_REGULATION_OF_NOTC H4_SIGNALING	53	0.65	2.32	4.46E-08	1.90E-06	1.51E-06	2771
PID_IL12_2PATHWAY	60	0.54	1.95	4.29E-05	0.0007	0.0006	1169
BIOCARTA_IL12_PATHWAY	19	0.67	1.91	0.001	0.0103	0.0082	1013
REACTOME_GENE_AND_PROTEIN_EXPRESSION_ BY_JAK_STAT_SIGNALING_AFTER_INTERLEUKI N_12_STIMULATION	31	0.57	1.84	0.001	0.0144	0.0114	3381
PID_IL12_STAT4_PATHWAY	32	0.56	1.80	0.003	0.0232	0.0184	1171
REACTOME_SIGNALING_BY_NOTCH	178	0.41	1.78	8.17E-06	0.0001	0.0001	2503
REACTOME_MAPK6_MAPK4_SIGNALING	82	0.46	1.78	0.0002	0.0025	0.0020	3275
WP_IL18_SIGNALING_PATHWAY	250	0.37	1.71	5.25E-06	0.0001	9.57E-05	1774
REACTOME_SIGNALING_BY_NOTCH4	78	0.44	1.70	0.001	0.0104	0.0083	2607
PID_IL23_PATHWAY	35	0.52	1.70	0.005	0.0359	0.0286	2710
WP_IL1_AND_MEGAKARYOCYTES_IN_OBESITY	24	0.56	1.69	0.007	0.0446	0.0354	1023
REACTOME_TCF_DEPENDENT_SIGNALING_IN_R ESPONSE_TO_WNT	171	0.31	1.34	0.007	0.0463	0.0367	1844
KEGG_TGF_BETA_SIGNALING_PATHWAY	81	-0.44	-1.61	0.006	0.0386	0.0306	2576
REACTOME_DISEASES_OF_GLYCOSYLATION	109	-0.43	-1.64	0.0007	0.0071	0.0057	1554
WP_REGULATION_OF_WNT_BCATENIN_SIGNALING_BY_SMALL_MOLECULE_COMPOUNDS	16	-0.68	-1.81	0.008	0.0478	0.0379	2704

GSEA, Gene Set Enrichment Analysis

3.8 Differential Expression Validation and Diagnostic Value Analysis of Hub Genes

(A) Differential expression analysis of hub genes glaucoma and control between samples. Pink-purple indicates control samples, orange-red indicates samples. glaucoma Statistical significance: ns $(p \ge 0.05)$, * (p <0.05), ** (p < 0.01), *** (p < 0.001). (B-D) ROC curve analysis for hub genes: SEC23A, BET1, and ARCN1 (B); COPB2, VCP, and UBC (C); SEC61B (D). AUC values between 0.7-0.9 indicate moderate diagnostic accuracy, while values between 0.5-0.7 suggest limited diagnostic potential. ROC: Receiver Operating Characteristic; AUC: Area Under the Curve; TPR: True Positive Rate; FPR: False Positive

To verify the transcriptional profiles of the hub genes, we performed a comparative assessment glaucoma between and healthy control specimens using the consolidated combining GSE2378 and GSE9944. differential expression evaluation (Figure 8A) revealed heterogeneous significance patterns across the core gene set. Three transcripts, ARCN1, VCP, and UBC, demonstrated profound expression disparities (p < 0.001), whereas three additional genes, SEC23A, COPB2, and SEC61B, showed considerable transcriptional differences (p < 0.01) between patients with glaucoma and

healthy controls.

We assessed the diagnostic capabilities of these hub genes using ROC curve analysis using the "pROC" package. The results (Figure 8B–D) indicated that six hub genes—SEC23A, ARCNI, COPB2, VCP, UBC, and SEC61B—demonstrated a moderate level of diagnostic accuracy, as evidenced by the AUC values ranging from 0.7 to 0.9. In contrast, BET1 showed limited diagnostic utility, with AUC values between 0.5 and 0.7.

3.9 Immune Cell Infiltration Analysis in Glaucoma

(A) Differential abundance of immune cell populations between glaucoma and control samples. Pink-purple indicates control samples, orange-red indicates glaucoma samples. (B) Correlation heatmap showing relationships between significantly altered immune cell populations. (C) Bubble plot denicting correlations between hub genes and immune cell infiltration levels. Orange indicates positive correlation, blue indicates negative correlation, with color intensity reflecting correlation strength. Statistical significance: ns ($p \ge 0.05$), * (p < 0.05), ** (p < 0.01), *** (p < 0.001). Correlation strength interpretation: |r| < 0.3(negligible), 0.3 - 0.5(weak), 0.5 - 0.8(moderate), > 0.8(strong). ssGSEA: single-sample Gene Set Enrichment Analysis. Through ssGSEA methodology, we evaluated immune subset distributions across 28 distinct cell types within the consolidated dataset. Comparative analysis identified significant differences (p < 0.05) in eight specific immune populations between diseased and control specimens (Figure 9A). These altered cellular

subsets encompassed activated CD4+ T cells, dendritic cell populations, CD56+ bright NK cells, myeloid suppressors, monocytic cells, neutrophilic infiltrates, Th1 populations, and Th17 subsets.

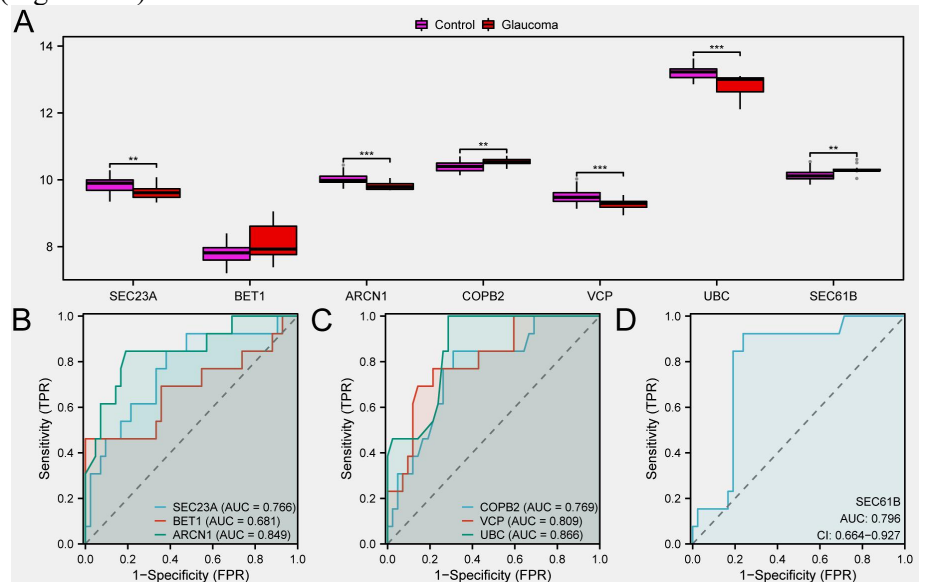


Figure 8. Expression Validation and Diagnostic Potential of Hub Genes.

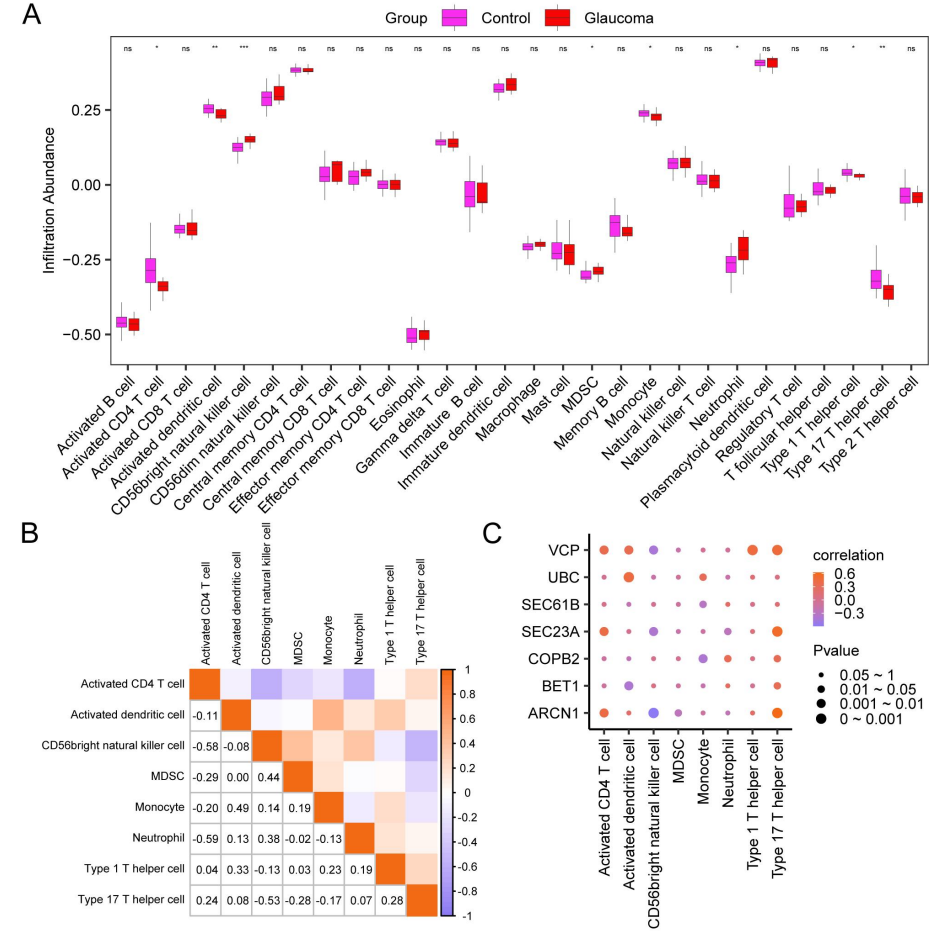


Figure 9. Analysis of Immune Cell Infiltration Patterns in Glaucoma.

We subsequently performed a correlation assessment across the eight immune cell subsets that exhibited remarkable alterations (Figure 9B). Our findings demonstrated the most robust positive association between monocytes and activated dendritic cells (r = 0.49), whereas the strongest inverse relationship was observed between neutrophils and activated CD4+ T cells (r = -0.59).

Additionally, we explored the relationships between the seven key genes and the patterns of immune cell infiltration, which revealed significant correlations (Figure 9C). Importantly, activated CD4 T cells positively correlated with all seven key genes, suggesting that these genes may contribute toward glaucoma pathogenesis by affecting the function of CD4+ T cells and modulating immune responses.

4. Discussion

Recently, glaucoma has emerged as a leading cause of irreversible blindness, primarily due to the degeneration of RGCs. This condition involves complex pathological mechanisms, particularly astrocyte dysfunction, which is vital for maintaining retinal health. To our knowledge, this represents the first systematic investigation of glycosylation machinery in human glaucoma astrocytes. Our study aimed to explore the roles of glycosylation-related DEGs in glaucoma. We identified 42 glycosylation-related DEGs, including seven key hub genes: SEC23A, BET1, ARCN1, COPB2, VCP, UBC, and SEC61B. These genes are crucial for protein trafficking and the regulation of secretory pathways. Functional enrichment analyses revealed significant involvement in glycoprotein metabolic processes and inflammatory pathways, with GSEA underscoring the important roles of Wnt/β-catenin signaling and IL-23 pathways. Additionally, our findings showed that six of the central genes had strong potential for diagnostic use. Our analysis suggests a potential association between astrocyte glycosylation dysfunction and immune responses in glaucoma. The positive correlations between all hub genes and activated CD4+ T cell infiltration patterns indicate that glycosylation-related processes may participate in immune microenvironment alterations during disease progression.

Valosin-containing protein (VCP)/p97 is a crucial AAA+ ATPase that serves critical functions in protein quality control, ER stress resolution, and ubiquitin-dependent degradation

of misfolded proteins[29-30]. These mechanisms essential for neuronal maintenance. particularly given neurons' limited regenerative capacity. In conditions like amyotrophic lateral sclerosis and Alzheimer's disease, **VCP** dysfunction impairs the removal of toxic including aggregates tau and TDP-43, exacerbating cellular toxicity and inflammatory responses [31]. In glaucoma pathology, where intraocular pressure. elevated ischemic conditions, and aging converge, VCP function compromised may become [32]. dysfunction can result in the buildup of detrimental proteins like crystallin and amyloid-β, alongside enhanced ER stress. Furthermore, compromised VCP activity may disrupt microglia-astrocyte communication, amplifying neuroinflammatory cascades that promote RGC degeneration.

The ubiquitin-conjugating enzyme (UBC) plays a critical role in the ubiquitin-proteasome pathway, which is essential for the degradation and regulation of intracellular proteins (Pickart, 2001). This enzyme tags target proteins with ubiquitin, signaling them for degradation by the proteasome, thereby helping maintain protein balance within the cell[33]. UBC is widely distributed across diverse tissue types within the organism, with a particularly important function in the retina, wherein it helps preserve the integrity of retinal cells[34]. Alzheimer's and Parkinson's diseases involve progressive accumulation of misfolded proteins amyloid-beta and alpha-synuclein, leading to neuronal damage and cell death[35]. UBC is vital for maintaining protein equilibrium and regulating inflammatory responses in retinal cells.UBC's function in degrading misfolded proteins and managing cellular stress responses indicates its potential importance in glaucoma pathogenesis.

SEC23A functions as an essential element within the COPII transport system, facilitating protein movement between ER and Golgi compartments, critical for neuronal integrity[36]. During glaucoma pathogenesis, SEC23A impairment may compromise neuroprotective chaperone trafficking such as heat shock protein 70 and transmembrane receptors. This potential disruption could cause misfolded proteins, like crystallins, to accumulate in the ER, which in turn triggers a specific apoptotic pathway involving protein kinase R-like ER kinase, eukaryotic translation initiation factor 2-alpha,

and activating transcription factor 4 in RGCs. Additionally, the possible impaired secretion of cytokines dependent on COPII worsens the polarization of microglia towards the M1 phenotype and intensifies neuroinflammatory processes. Current research has demonstrated that SEC23A deficiency results in impaired autophagosome-lysosome fusion, allowing harmful aggregates similar to α-synuclein to persist [37]. These potential combined issues of proteotoxicity and inflammation highlight SEC23A critical factor as a in the neurodegeneration seen in glaucoma, suggesting that it could be a target for new therapies, such as ER stress modulators such as 4-phenylbutyric acid, or gene therapies aimed at the COPII pathway.

Our ssGSEA analysis revealed alterations in immune-related gene expression signatures within glaucoma astrocyte samples, which were derived from purified optic nerve head astrocytes and represent indirect inference based on immune-associated gene set enrichment. The analysis showed enrichment of gene signatures typically associated with activated CD4+ T cells, dendritic cells, and neutrophils, reflecting the molecular responsiveness of astrocytes to immune signals and inflammatory states in the glaucomatous environment. We observed a robust positive association between monocyte and activated dendritic cell gene signatures (r = 0.49), and all seven hub genes were positively correlated with activated CD4+ T cell-associated gene signatures. These findings suggest that immune responses may disrupt astrocyte glaucoma glycosylation processes during progression. Inflammatory signals potentially interfere with normal protein processing in astrocytes, compromising their neuroprotective functions and contributing to RGC degeneration. [38-40]. While our results primarily reflect the immune-responsive molecular capacity of astrocytes rather than the actual abundance or spatial distribution of immune cells within tissues, they support the growing evidence that immune dysregulation contributes to glaucomatous neurodegeneration. Future validation through immunohistochemistry, flow cytometry, and functional experiments will be essential to comprehensively elucidate the multilevel mechanisms of glaucoma-related immune regulation.

Our study has several limitations. First, we analyzed microarray data from cultured

astrocytes obtained from post-mortem tissues, which may not fully reflect the in vivo cellular state. Second, the bulk RNA sequencing approach cannot distinguish gene expression changes in different astrocyte subpopulations. focusing specifically glycosylation-related genes may have excluded other important pathways involved in glaucoma pathogenesis. Fourth, our findings are based on computational analysis and require experimental validation in independent patient cohorts. Finally, the mechanistic relationships between identified glycosylation genes and immune cell infiltration need further investigation through functional studies.

In summary, our study identified critical glycosylation-related genes dysregulated in glaucoma astrocytes. Our findings suggest that dysfunction astrocvte glycosylation contribute to RGC degeneration in glaucoma pathogenesis, while this glycosylation impairment appears to be associated with immune dysregulation. These results indicate that glycosylation defects and immune responses may be interconnected processes that together contribute to glaucoma progression. identified hub genes provide potential therapeutic targets for interventions aimed at restoring both protein processing and immune balance in glaucoma treatment.

Acknowledgments

This work was supported by the Shenzhen Science and Technology Innovation Program (JCYJ20190809163205531).

CRediT Authorship Contribution Statement

Dingqiao Wang: Writing-original draft, Conceptualization. Minyi Zhu: Methodology, Data curation. Peidong Yuan: Data curation. Yiyu Xie: Data curation. Bingying Lin: Investigation. Hongzhi Yuan: Writing – review and editing, Supervision.

References

- [1] Davis BM, Crawley L, Pahlitzsch M, Javaid F, Cordeiro MF. Glaucoma: the retina and beyond. Acta Neuropathol. 2016;132(6):807-826.
- [2] Zhao GL, Zhou H, Guo YH, et al. Modulation of Rac1/PAK1/connexin43-mediated ATP release from astrocytes contributes to retinal ganglion cell survival in experimental

- glaucoma. Glia. 2023;71(6):1502-1521.
- [3] Salkar A, Wall RV, Basavarajappa D, et al. Glial Cell Activation and Immune Responses in Glaucoma: A Systematic Review of Human Postmortem Studies of the Retina and Optic Nerve. Aging Dis. 2024;15(5):2069-2083.
- [4] Jayaprakash NG, Surolia A. Role of glycosylation in nucleating protein folding and stability. Biochem J. 2017;474(14):2333-2347.
- [5] Kang H, Han AR, Zhang A, Jeong H, Koh W, Lee JM, Lee H, Jo HY, Maria-Solano MA, Bhalla M, Kwon J, Roh WS, Yang J, An HJ, Choi S, Kim HM, Lee CJ. GolpHCat (TMEM87A), a unique voltage-dependent cation channel in Golgi apparatus, contributes to Golgi-pH maintenance and hippocampus-dependent memory. Nat Commun. 2024 Jul 11;15(1):5830.
- [6] Shafi S, Singh A, Gupta P, et al. Deciphering the Role of Aberrant Protein Post-Translational Modification in the Pathology of Neurodegeneration. CNS Neurol Disord Drug Targets. 2021;20(1):54-67.
- [7] Gonatas NK, Stieber A, Gonatas JO. Fragmentation of the Golgi apparatus in neurodegenerative diseases and cell death. J Neurol Sci. 2006;246(1-2):21-30.
- [8] Hernandez MR, Agapova OA, Yang P, Salvador-Silva M, Ricard CS, Aoi S. Differential gene expression in astrocytes from human normal and glaucomatous optic nerve head analyzed by cDNA microarray. Glia. 2002 Apr 1;38(1):45-64.
- [9] Kompass KS, Agapova OA, Li W, Kaufman PL, Rasmussen CA, Hernandez MR. Bioinformatic and statistical analysis of the optic nerve head in a primate model of ocular hypertension. BMC Neurosci. 2008 Sep 26;9:93.
- [10] Nikolskaya T, Nikolsky Y, Serebryiskaya T, Zvereva S, Sviridov E, Dezso Z, Rahkmatulin E, Brennan RJ, Yankovsky N, Bhattacharya SK, Agapova O, Hernandez MR, Shestopalov VI. Network analysis of human glaucomatous optic nerve head astrocytes. BMC Med Genomics. 2009 May 9;2:24.
- [11] Lukas TJ, Miao H, Chen L, Riordan SM, Li W, Crabb AM, Wise A, Du P, Lin SM, Hernandez MR. Susceptibility to glaucoma: differential comparison of the astrocyte

- transcriptome from glaucomatous African American and Caucasian American donors. Genome Biol. 2008;9(7):R111.
- [12] Barrett T, Wilhite SE, Ledoux P, Evangelista C, Kim IF, Tomashevsky M, Marshall KA, Phillippy KH, Sherman PM, Holko M, Yefanov A, Lee H, Zhang N, Robertson CL, Serova N, Davis S, Soboleva A. NCBI GEO: archive for functional genomics data sets--update. Nucleic Acids Res. 2013 Jan; 41 (Database issue): D991-995.
- [13] Stelzer G, Rosen N, Plaschkes I, Zimmerman S, Twik M, Fishilevich S, Stein TI, Nudel R, Lieder I, Mazor Y, Kaplan S, Dahary D, Warshawsky D, Guan-Golan Y, Kohn A, Rappaport N, Safran M, Lancet D. The GeneCards Suite: From Gene Data Mining to Disease Genome Sequence Analyses. Curr Protoc Bioinformatics. 2016 Jun 20;54:1.30.1-1.30.33.
- [14] Chen L, Ling Y, Yang H. Comprehensive Analysis of the Potential Prognostic Value of 11 Glycosylation-Related Genes in Head and Neck Squamous Cell Carcinoma and Their Correlation with PD-L1 Expression and Immune Infiltration. J Oncol. 2022 Apr 14;2022:2786680.
- [15] Leek JT, Johnson WE, Parker HS, Jaffe AE, Storey JD. The sva package for removing batch effects and other unwanted variation in high-throughput experiments. Bioinformatics. 2012 Mar 15;28(6):882-883.
- [16] Ritchie ME, Phipson B, Wu D, Hu Y, Law CW, Shi W, Smyth GK. limma powers differential expression analyses for RNA-sequencing and microarray studies. Nucleic Acids Res. 2015 Apr 20;43(7):e47.
- [17] Ben Salem K, Ben Abdelaziz A. Principal Component Analysis (PCA). Tunis Med. 2021 Avril;99(4):383-389.
- [18] Yu G, Wang LG, Han Y, He QY. clusterProfiler: an R package for comparing biological themes among gene clusters. OMICS. 2012 May;16(5):284-287.
- [19] Mi H, Muruganujan A, Ebert D, Huang X, Thomas PD. PANTHER version 14: more genomes, a new PANTHER GO-slim and improvements in enrichment analysis tools. Nucleic Acids Res. 2019 Jan 8;47(D1):D419-D426.
- [20] Kanehisa M, Goto S. KEGG: kyoto encyclopedia of genes and genomes. Nucleic Acids Res. 2000 Jan 1;28(1):27-30.

- [21] Luo W, Brouwer C. Pathview: an R/Bioconductor package for pathway-based data integration and visualization. Bioinformatics. 2013 Jul 15;29(14):1830-1831.
- [22] Yu G, Wang LG, Han Y, He QY. clusterProfiler: an R package for comparing biological themes among gene clusters. OMICS. 2012 May;16(5):284-287.
- [23] Shannon P, Markiel A, Ozier O, Baliga NS, Wang JT, Ramage D, Amin N, Schwikowski B, Ideker T. Cytoscape: a software environment for integrated models of biomolecular interaction networks. Genome Res. 2003 Nov;13(11):2498-2504.
- [24] Chin CH, Chen SH, Wu HH, Ho CW, Ko MT, Lin CY. cytoHubba: identifying hub objects and sub-networks from complex interactome. BMC Syst Biol. 2014;8 Suppl 4(Suppl 4):S11.
- [25] Zhou KR, Liu S, Sun WJ, Zheng LL, Zhou H, Yang JH, Qu LH. ChIPBase v2.0: decoding transcriptional regulatory networks of non-coding RNAs and protein-coding genes from ChIP-seq data. Nucleic Acids Res. 2017 Jan 4;45(D1):D43-D50.
- [26] Li JH, Liu S, Zhou H, Qu LH, Yang JH. starBase v2.0: decoding miRNA-ceRNA, miRNA-ncRNA and protein-RNA interaction networks from large-scale CLIP-Seq data. Nucleic Acids Res. 2014 Jan;42(Database issue):D92-97.
- [27] Robin X, Turck N, Hainard A, Tiberti N, Lisacek F, Sanchez JC, Müller M. pROC: an open-source package for R and S+ to analyze and compare ROC curves. BMC Bioinformatics. 2011 Mar 17;12:77.
- [28] Xiao B, Liu L, Li A, Xiang C, Wang P, Li H, Xiao T. Identification and Verification of Immune-Related Gene Prognostic Signature Based on ssGSEA for Osteosarcoma. Front Oncol. 2020 Dec 15;10:607622.
- [29] Aguiar BG, Dumas C, Maaroufi H, Padmanabhan PK, Papadopoulou B. The AAA + ATPase valosin-containing protein (VCP)/p97/Cdc48 interaction network in Leishmania. Sci Rep. 2020;10(1):13135.
- [30] Shah PP, Beverly LJ. Regulation of VCP/p97 demonstrates the critical balance between cell death and epithelial-mesenchymal transition (EMT) downstream of ER stress. Oncotarget. 2015;6(19):17725-17737.
- [31] Pontifex CS, Zaman M, Fanganiello RD,

- Shutt TE, Pfeffer G. Valosin-Containing Protein (VCP): A Review of Its Diverse Molecular Functions and Clinical Phenotypes. Int J Mol Sci. 2024 May 22;25(11):5633.
- [32] Hasegawa T, Ikeda HO, Gotoh N, Iida K, Iwai S, Nakano N, Kakizuka A, Tsujikawa A. Effect of VCP modulators on gene expression profiles of retinal ganglion cells in an acute injury mouse model. Sci Rep. 2020 Mar 6;10(1):4251.
- [33] Dikic I, Schulman BA. An expanded lexicon for the ubiquitin code. Nat Rev Mol Cell Biol. 2023 Apr;24(4):273-287.
- [34] Mirza S, Plafker KS, Aston C, Plafker SM. Expression and distribution of the class III ubiquitin-conjugating enzymes in the retina. Mol Vis. 2010 Nov 18;16:2425-2437.
- [35] Marsh SE, Blurton-Jones M. Examining the mechanisms that link β-amyloid and α-synuclein pathologies. Alzheimers Res Ther. 2012 Apr 30;4(2):11.
- [36] Khoriaty R, Hesketh GG, Bernard A, Weyand AC, Mellacheruvu D, Zhu G, Hoenerhoff MJ, McGee B, Everett L, Adams EJ, Zhang B, Saunders TL, Nesvizhskii AI, Klionsky DJ, Shavit JA, Gingras AC, Ginsburg D. Functions of the COPII gene paralogs SEC23A and SEC23B are interchangeable in vivo. Proc Natl Acad Sci U S A. 2018 Aug 14;115(33):E7748-E7757.
- [37] Sun Z, Zeng B, Liu D, Zhao Q, Wang J, Rosie Xing H. S100A8 transported by SEC23A inhibits metastatic colonization via autocrine activation of autophagy. Cell Death Dis. 2020 Aug 6;11(8):650.
- [38] Chen H, Cho KS, Vu THK, Shen CH, Kaur M, Chen G, Mathew R, McHam ML, Fazelat A, Lashkari K, Au NPB, Tse JKY, Li Y, Yu H, Yang L, Stein-Streilein J, Ma CHE, Woolf CJ, Whary MT, Jager MJ, Fox JG, Chen J, Chen DF. Commensal microflora-induced T cell responses mediate progressive neurodegeneration in glaucoma. Nat Commun. 2018 Aug 10;9(1):3209.
- [39] Tezel G. The immune response in glaucoma: a perspective on the roles of oxidative stress. Exp Eye Res. 2011 Aug;93(2):178-186.
- [40] Wang L, Wei X. T Cell-Mediated Autoimmunity in Glaucoma Neurodegeneration. Front Immunol. 2021 Dec 16;12:803485.